www.MaterialsViews.com

ADVANCED
FUNCTIONAL
MATERIALS
www.afm-journal.de

FULL PAPER

Universal Electron Injection Dynamics at Nanointerfaces in Dye-Sensitized Solar Cells

Lei Wang, Hai-Yu Wang,* Hong-Hua Fang, Hai Wang, Zhi-Yong Yang, Bing-Rong Gao, Qi-Dai Chen, Wei Han, and Hong-Bo Sun*

Initial nanointerfacial electron transfer dynamics are studied in dye-sensitized solar cells (DSSCs) in which the free energy and kinetics vary over a broad range. Surprisingly, it is found that the decay profiles, reflecting the electron transfer behavior, show a universal shape despite the different kinds of dye and semiconductor nanocrystalline films, even across different device types. This renews intuitive knowledge about the electron injection process in DSSCs. In order to quantitatively comprehend the universal behavior, a static inhomogeneous electronic coupling model with a Gaussian distribution of local injection energetics is proposed in which only the electron injection rate is a variant. It is confirmed that this model can be extended to CdSe quantum dot-sensitized films. These unambiguous results indicate exactly the same physical distribution in electron injection process of different sensitization films, providing limited simple and important parameters describing the electron injection process including electronic coupling constant and reorganization energy. The results provide insight into photoconversion physics and the design of optimal metal-free organic dye-sensitized photovoltaic devices by molecular engineering.

1. Introduction

Dye-sensitized solar cells (DSSCs) are efficient, low-cost molecular photovoltaic devices.[1] Since Grätzel and co-workers reported the first solar cell devices based on TiO_2 nanocrystalline films sensitized with a ruthenium-based complex (RuN3) in the early 1990s, the power conversion efficiency of DSSCs has reached over 11%.[2] The mechanism for light-to-electrical energy conversion in DSSCs is considered to be controlled by a series of charge-transfer processes (**Figure 1**a),[3] which to a large extent determine device performance. Charge transfer occurs at nanointerfaces formed due to the adhesion of dyes to metal oxide nanoparticle surfaces. Measuring the electron injection kinetics is essential for designing nanointerfaces that are favorable for charge injection[4] and has thus become a subject of intense research. Experimentally, the dynamics have been observed to be quite complex and inhomogeneous; in detail, the electron transfer is strongly nonexponential, and occurs over a broad timescale from sub-100 femtoseconds to tens of picoseconds. For ruthenium (Ru)-based dyes, the ultrafast electron transfer is thought to take place from the initially-excited singlet state, while the slow process is from the triplet state.[5]

In contrast to natural photosynthesis, in which the complex charge separation is dynamically controlled by protein motion,[6] the electron injection dynamics in DSSCs are mainly controlled by static inhomogeneity, such as the spatial heterogeneities of the metal oxide surfaces and the inhomogeneous electronic coupling between the dye molecules and the nanoscale surface roughness.[4] Many systems have been studied previously, including various dyes and metal oxides.[7–11] Because the surface properties of nanocrystals are strongly dependent on preparation procedure and surrounding solvent molecules, the inhomogeneous kinetics may vary from system to system.[12] Due to the lack of unifying criteria, it is difficult to directly compare the electron injection processes between these systems.

Inspired by our previous study on photo-electron conversion dynamics in proteins, where the complex electron transfer kinetics are controlled by the same protein dynamics,[6] we wondered whether there exists any universal law that governs charge transfer in DSSCs. To this end, we choose different metal-free organic dyes like C209, C213, and C215 (Figure 1b) as sensitizer, because the use of metal-free organic dyes has lately become more and more attractive.[13–15] All of these are donor–π-conjugated linker–acceptor (D-π-A) dyes, employing identified electron donors (dihexyloxy-substituted triphenyl-amine) and acceptors (cyanoacrylic acid) in combination with different π-conjugated linkers– furan, thiophene, and selenophene, respectively. The different five-member heterocycle linker leads to a red shift in absorption and enhancement in molar extinction coefficient with decreased electronegativity of heteroatom (O > S > Se). In conjunction with an

L. Wang, Prof. H.-Y. Wang, H.-H. Fang, H. Wang,
Z.-Y. Yang, B.-R. Gao, Dr. Q.-D. Chen, Prof. H.-B. Sun
State Key Laboratory on Integrated Optoelectronics
College of Electronic Science and Engineering
Jilin University
2699 Qianjin Street, Changchun, 130012, P. R. China
E-mail: haiyu_wang@jlu.edu.cn; hbsun@jlu.edu.cn
H. Wang, Z.-Y. Yang, Prof. W. Han, Prof. H.-B. Sun
College of Physics
Jilin University
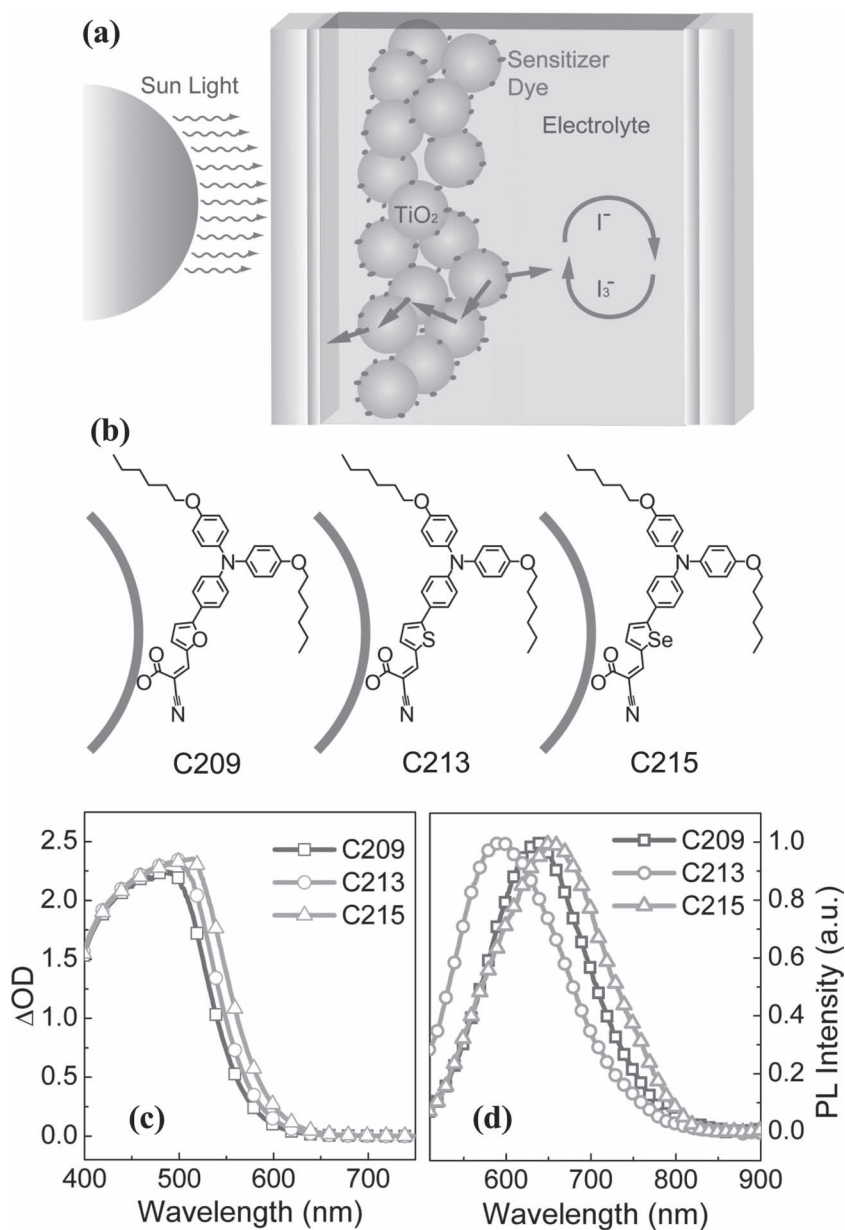119 Jiefang Road, Changchun, 130023, P. R. China

Figure 1. a) Schematic view of the series of charge transfer processes in dye-sensitized solar cells. b) Molecular structures, c) steady-state ΔOD spectra, and, d) emission spectra of the three kinds of organic dye sensitized devices.

shape after the time axis has been scaled up or down. The behavior is interpreted by a nanointerface diffusion model that is built using a series of purposely designed experiments, and further confirmed by application to earlier reports. We also discuss the applicability of this model, and find it can be extended to CdSe quantum dot-sensitized films. These results demonstrate that the seemingly complex electron transfer processes in varied species of dyes and device structures are actually governed by the same law, which can facilitate understanding of the photoconversion behavior and allow improvement of the performance of DSSCs.

2. Results and Discussion

2.1. Steady-State Absorption and Photoluminescence

Shown in Figure 1c are the steady-state ΔOD spectra of the three kinds of organic dye sensitized devices. Because these DSSCs usually contain many chemical complexities – including an iodide/iodine redox couple and additional additives in electrolyte – the steady state ΔOD spectra are more suitable to characterize the absorption of dyes adsorbed on metal oxides, in which the contribution of substrates and other components in electrolyte is subtracted. To achieve high efficiency, these devices need to adsorb as many dyes as possible. We see that all the ΔOD spectra are saturated below 500 nm. Red shifts of the absorption edges are also observed, in order of magnitude C209, C213, and C215. In contrast, the PL peak is blue-shifted by about 0.18 eV for C213 in the emission spectrum (Figure 1d). As presented in **Table 1**, in solution the lowest unoccupied molecular orbital (LUMO) of these dyes decreases with the magnitude of red shift, while the highest occupied molecular orbital (HOMO) remains the same. This variance between the absorption and emission implies that the electron injection in the devices may occur in the excited state of C213 dye, in which

acetonitrile-based electrolyte, these dyes exhibit high external quantum efficiencies (EQE, approximately 90%) and power conversion efficiencies (approximately 7%). The molecular structures also provided an opportunity to systemically study the inherent charge transfer properties in devices. For experimental studies, we employed femtosecond transient absorption (TA) spectroscopy and fluorescence up-conversion. The former provides information about the ground-state recovery process while the latter reveals the pure excited-state dynamics. As a result, interestingly and surprisingly we find that the dynamical decay profile resulting from the electron transfer process in all the metal-free organic dye-sensitized devices show a universal

Table 1. Molecular orbitals of the dyes.

	HOMO[a] [eV]	LUMO[a] [eV]	Modified LUMO [eV]
C209	−5.09	−3.35	−3.60
C213	−5.09	−3.42	−3.49
C215	−5.09	−3.43	−3.68

[a]Ref. [13].

www.MaterialsViews.com

ADVANCED
FUNCTIONAL
MATERIALS
www.afm-journal.de

FULL PAPER

the injection position is higher about 0.18 eV than its LUMO in solution. We also note that the LUMO levels are usually slightly decreased in film compared to in solution, for example by about 0.3 eV in the case of C218 dye.[13,14] Thus, when we adopt the conduction band (CB) of TiO_2 in DSSCs at around 4.0 eV below the vacuum level,[3] the driving force of electron injection could be considered as the energy difference between the CB of the semiconductor and the excited states of the dyes.

2.2. The Transient Absorption Spectroscopy

To scrutinize the energetics and kinetic interplay in the three kinds of metal-free organic dyes, at first we used femtosecond transient absorption (TA) spectroscopy to study these systems in the visible and near infrared (NIR) region. **Figure 2** shows the time evolution transient spectra on the femtosecond to nanosecond timescale. In the sequence C209, C213, C215, a red shift is validated for the negative bleaching signal of absorption edges. This is in agreement with the steady-state spectra. The bleaching signals rise fast in the first 0.6 ps and then slowly to tens of picoseconds. The shape of the positive absorption signals gradually change; this is due to a serious spectral overlap in these regions, i.e., exited state absorption,

absorption of cation, and/or stimulated emission. As shown in Figure S1 (see the Supporting Information), the TA spectra of corresponding dye-sensitized Al_2O_3 films present a broad exited state absorption, which is superimposed on stimulated emission. The change of positive absorption shape can probably be ascribed to the overlapping signals between excited state and oxidation state, and the contribution of oxidation state is gradually red-shifted out of this window with the decreased electronegativity of heteroatoms. This makes it difficult to separate the initial electron injection process from other species, but according to the difference spectrum shown in **Figure 3**a, the positive absorption signal from 750 to 850 nm can be ascribed to the oxidation state of C213, since it is consistent with spectroelectrochemical measurements of oxidation state.[16] As shown in Figure 3b, the dynamics in this region presents a flat stage within the first 10 ps. A usual method to avoid this problem is subtracting the contribution of dye exited state absorption in the reference samples from the data of sensitized TiO_2 films.[12] In our case, the reference samples are dye-sensitized Al_2O_3 films. However, we found using this method would give a slower rise trace, with rise time of around 13 ± 2 ps, accompanied by a long decay within nanosecond timescale, and lead to a lower injection yield (approximately 79%), compared to the excited state decay to ground
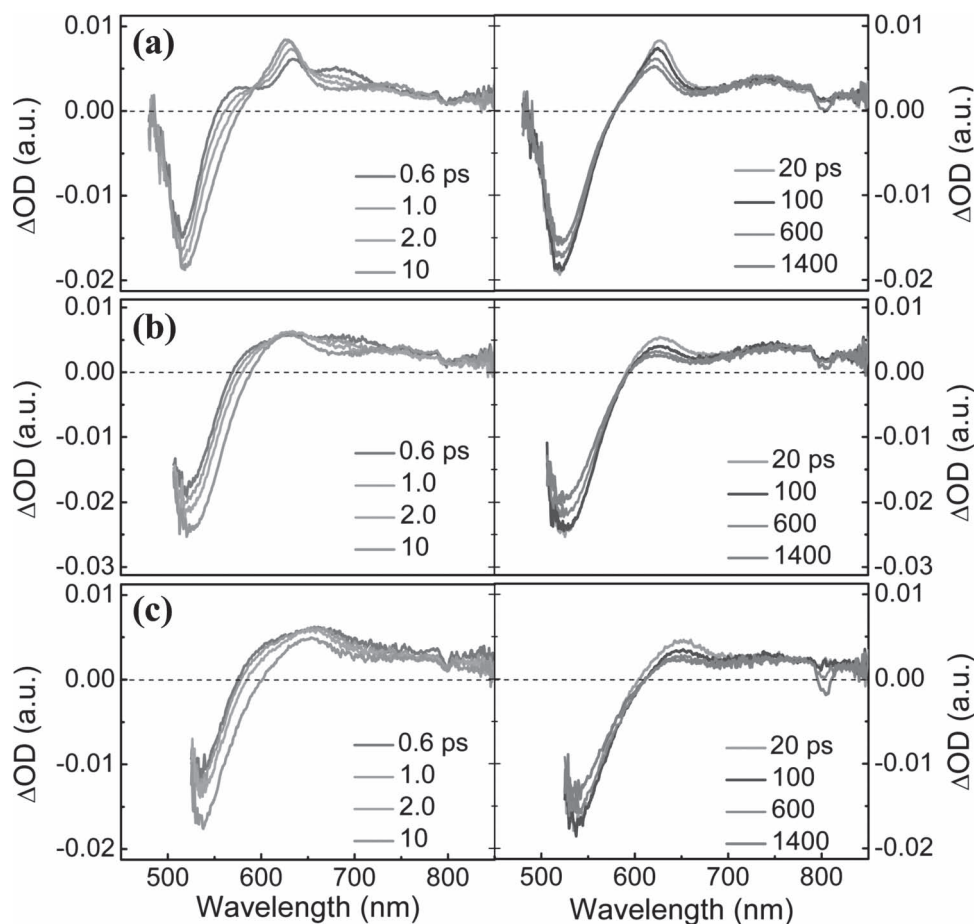

Figure 2. The time evolution transient absorption spectra of: a) C209, b) C213, and, c) C215 sensitized devices.
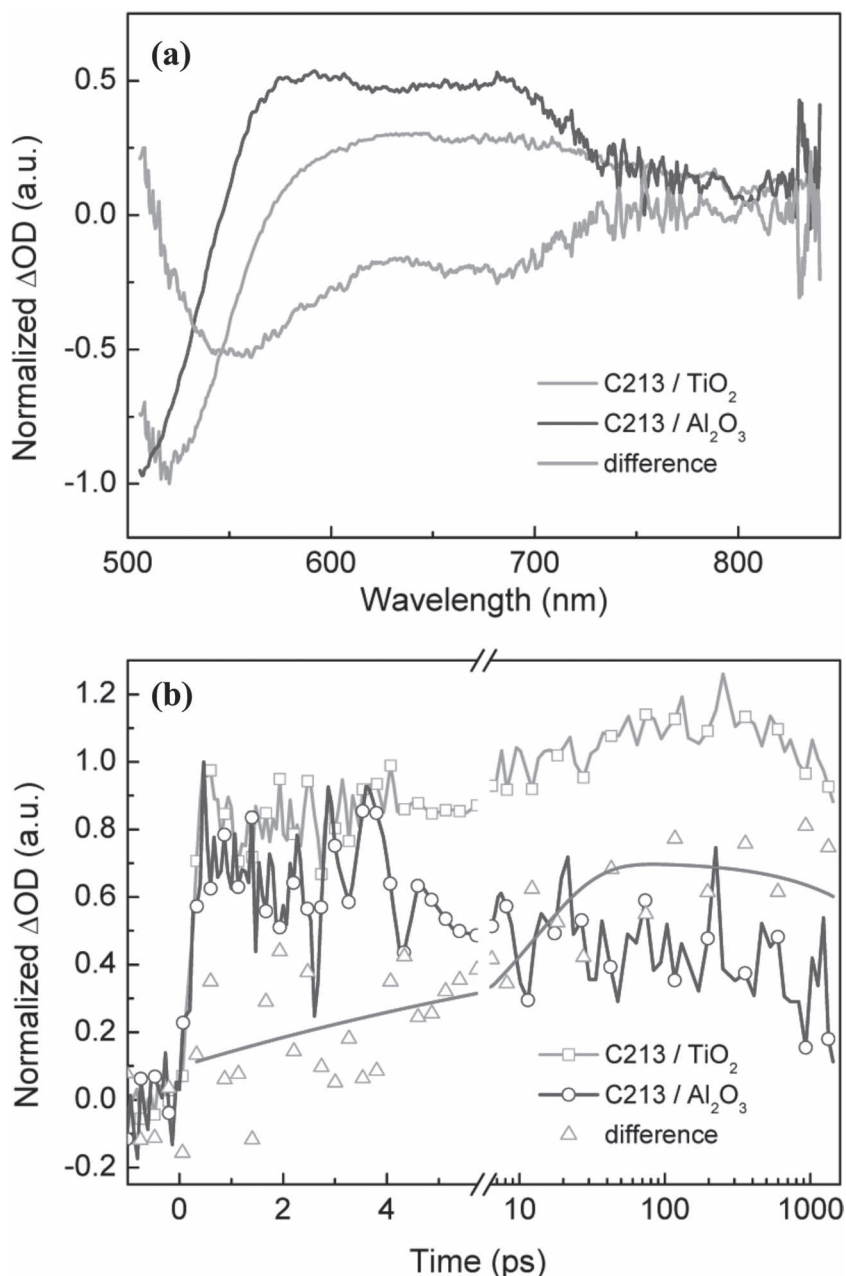
Figure 3. a) The normalized TA spectra for C213-sensitized TiO₂ (orange) and Al₂O₃ (blue) film at 0.6 ps. b) The TA dynamics at 750 nm for C213-sensitized TiO₂ (square) and Al₂O₃ (circle) film. The difference data are obtained by subtracting the contribution of Al₂O₃ film from TiO₂ film. The pink line in b represents the fit using exponential analysis.

2.3. Time-Resolved Photoluminescence Dynamics

Figure 4a shows the electron injection dynamics in these DSSCs measured by femtosecond fluorescence up-conversion. The dye-sensitized Al₂O₃ films are also measured, in which only recombination from photo-exited electron relaxed to the ground state is considered. This could help us to determine the electron injection yields. Multiple exponential analyses give values of electron injection yield for C209, C213, and C215 of 0.94, 0.99, and 0.85, respectively, which are in agreement with the EQE data (see Table S1 in the Supporting Information for details). This demonstrated that in these metal-free organic dye-sensitized devices, the time-resolved photoluminescence dynamics can be directly assigned to the interfacial electron injection. Interestingly, if we scale up (or down) the time axis by an appropriate value, taking C213 as a standard, these kinetics traces can perfectly overlap with each other, shown in Figure 4b. We believe this phenomenon arises from some mechanism, which implies a consistency in the nature of the electron injection process in DSSCs.

2.4. Theoretical Analysis and Modeling

To verify our speculation, an inhomogeneous distribution of free energy model was adopted. The scheme of this model is shown in **Figure 5**. In this model, the electron injection rate, $k(D)$, depends on the local shift D in the energies of the oxide acceptor states relative to excited state of the dye. Considering an exponential density of states $\exp(-D/E_0)$, where E_0 is a experimental energy coefficient varying between 60 and 200 meV, this is equivalent to a model based on distribution of electronic coupling, which gives $k(D)$ = $k(0)\exp(-2D/E_0)$.[4,17] Assuming D has a Gaussian distribution (average 0 and width Δ) and integrating over all possible values of D, the femtosecond fluorescence decay could be expressed as

$$N_e(t) = N_0 \int \rho(D) \exp[-k(D)t]\mathrm{d}(D) \tag{1}$$

In early work, such as that of Durrent and co-workers, the model has two parameters, $k(0)$ and Δ/E_0. The change of Δ/E_0 means the distribution of local shift D varies from system to system, considering E_0 to be constant.[12] From such a point of view, the traces cannot be overlapped by simple scaling of the time axis, because it is impossible that each sample has the

(around 61 ps). This method may be not suitable for metal-free organic dyes, since the recombination of these organic dyes is apparently faster than that of Ru-based dyes.[12,16] In this research, we focus on the interfacial electron transfer, so it is important to carry out ultrafast time-resolved photoluminescence spectroscopy, for example, femtosecond photoluminescence up-conversion, which gives direct access to the electron transfer dynamics occurring in the interface between the dye and metal oxides.

Materials
Views
www.MaterialsViews.com

ADVANCED
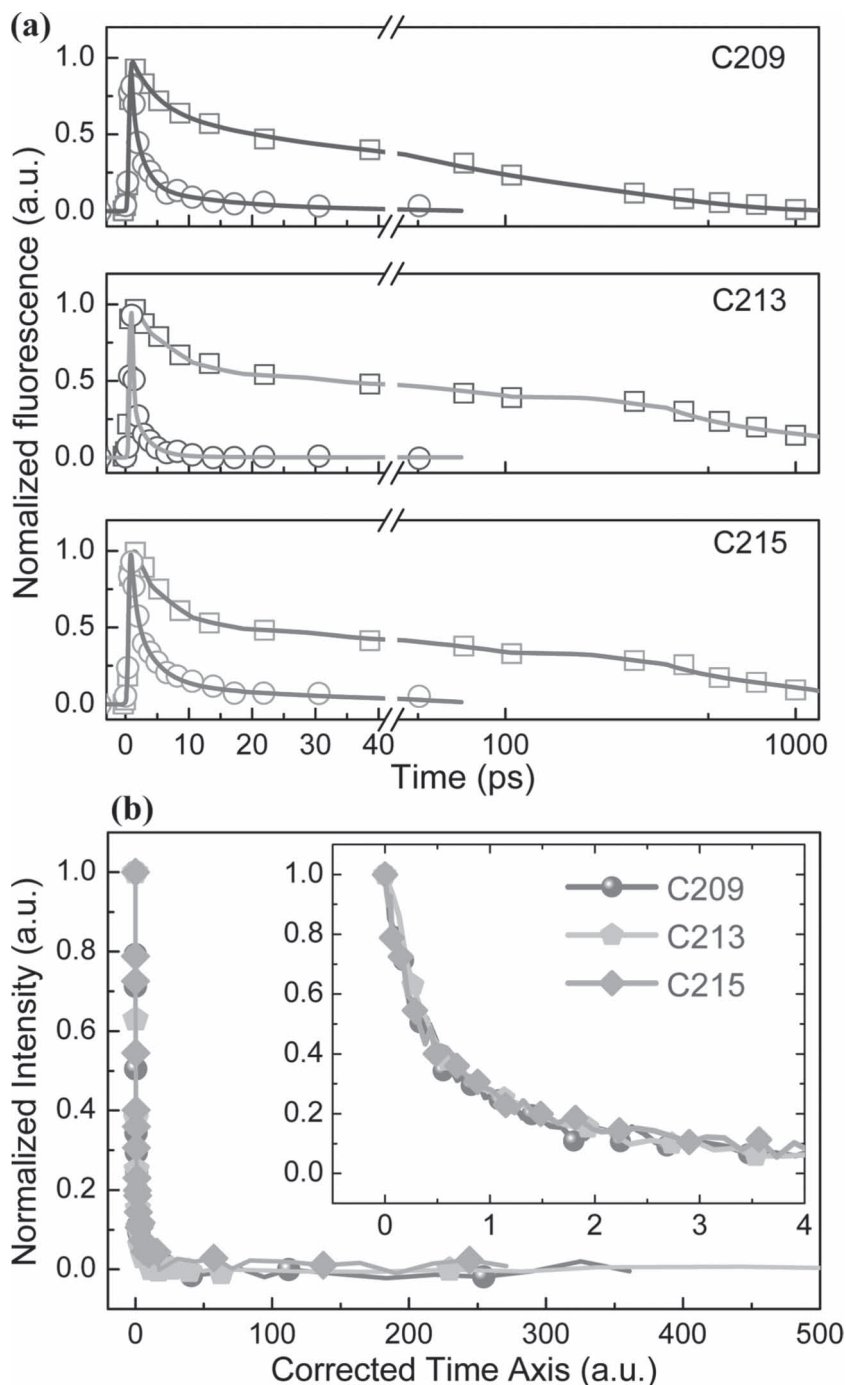FUNCTIONAL
MATERIALS
www.afm-journal.de

FULL PAPER

Figure 4. a) Normalized electron injection dynamics in DSSCs (circle) compared with dye-sensitized Al_2O_3 films (square). b) Kinetic traces overlap via scaling down the time axis by an appropriate value, taking C213 as a standard.

the same distribution. Fitting our results gives a value of $\Delta/E_0 = 1.5$ for all the kinetics ($k(0)$ for our samples is given in **Table 2**). We should point out that if one considers the distribution of electronic coupling to be due to the various spatial separations d of the donor and acceptor states, a similar conclusion will be obtained since $H(d) = H_0\exp(-\beta d)$. Therefore, the static distribution of the electronic coupling is the dominant factor governing the complex kinetics. This reflects the nature of dye adsorbing on the nanocrystal surface is similar distribution of electronic coupling and heterogeneities in semiconductor nanocrystalline films, rather than the different degree of energetic disorder.

From this point of view, we further investigated the electron injection dynamics reported by different groups. In that work, the dynamics are measured using a variety of techniques, and many kinds of dyes, namely: ZnTCPP,[7] H_2TCPP, Ru(dcbpy)$_2$(NCS)$_2$ and Ru-bpy complexes with different linkers length (named Rods 1–2)[8] are adopted to sensitize various semiconductor nanocrystals, such as TiO_2, ZnO,[9] SnO_2,[10] and In_2O_3[11] nanoparticles. It is remarkable that the model works well for all the decay curves, shown in **Figure 6**, notwithstanding the rate changes by more than two orders of magnitude (Table 2); applying the model to these data also gives $\Delta/E_0 = 1.5$. According to the obtained electron transfer rate, we noticed that the scaling constant of time axis that we previously found in Section 2.3 is consistent with the ratio of electron transfer rate. This point has been reflected in Equation 1, that is a timescale transform is equivalent to a change of rate. In all the investigated samples, only the electron injection rate is variable, keeping a same distribution of electronic coupling due to the same value of Δ/E_0. As a result of this concept, the universal dynamics strongly indicate that the interfacial electron transfer follows exactly the same physical process, which is essential and contingent upon the physical distribution, regardless of the type of dye-sensitized film, even for our measured DSSCs. In other words, the distribution of electronic coupling is almost the same, which exactly gives similar ratio, Δ/E_0, and the strength of average electronic coupling is different, which decides the electron injection rate, $k(0)$.

Recent reports on dye-sensitized size-selected ZnO colloids,[18] and CdSe nanocrystal-sensitized TiO_2 nanoparticles[19] and nanoparticulate films[20] also attracted our attention. Huss et al. and Robel et al. respectively demonstrated the influence of acceptor state density and donor potential on electron transfer by altering the acceptor nanocrystalline ZnO

same degree of energetic disorder. However, in our case, the samples have little difference in molecular structure and device constitution, providing an opportunity to systemically study the inherent charge transfer properties. According to the findings from time-resolved photoluminescence spectroscopy, we noticed that our result is also consistent with this model; that is, it will result in a unique decay shape when all DSSCs have

ADVANCED
FUNCTIONAL
MATERIALS
www.afm-journal.de
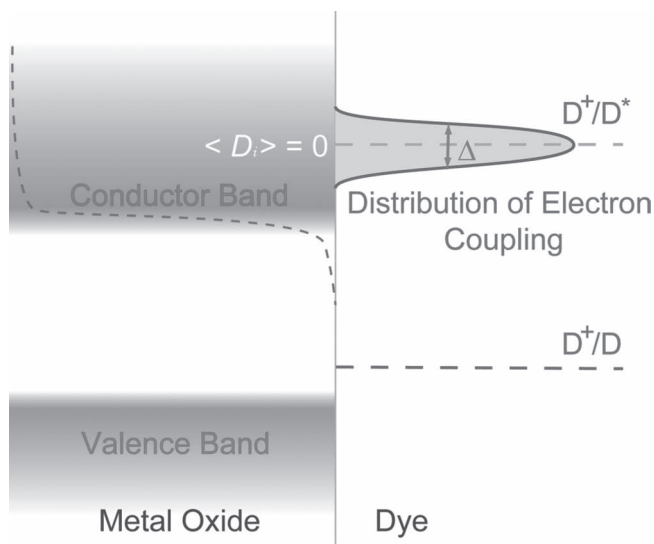
Materials
Views
www.MaterialsViews.com

Figure 5. The scheme of a static inhomogeneous electronic coupling model with a Gaussian distribution (width Δ) of local offsets (D) for local injection energetics.

and donor CdSe nanocrystals size in solution. These colloidal nanocrystal solution systems provide a relative simple platform for study the details in electron transfer reaction.[21–23] We found that the present model could not be directly application in the solution samples.[18] The main reason may be the different distribution of surface states in colloidal nanocrystal solution, which would lead to a smaller ratio Δ/E_0 compared to that in films. However, theoretically our model could be suitable for quantum dot (QD)-sensitized films. Kongkanand et al. studied the emission decay of CdSe QDs deposited on TiO$_2$ nanoparticulate films, which indicated the electron transfer process from the photoluminescence quenching.[20] So, we also prepared a CdSe QD-sensitized TiO$_2$ nanocrystalline film and measured the PL decay by time-correlated single-photon counting (TCSPC). The QD size was approximately 3.0 nm, estimated as described elsewhere,[24] and the absorption and emission spectra are present in Figure S2 (see the Supporting

Table 2. Driving force and electron injection rate constants.

Sample	ΔG [eV]	k_{ET} [ps^{-1}]	Δ/E_0
C209/TiO$_2$	−0.4	0.59 ± 0.02	1.5
C213/TiO$_2$	−0.51	1.59 ± 0.03	1.5
C215/TiO$_2$	−0.32	0.41 ± 0.02	1.5
CdSe QD (3.0 nm)/TiO$_2$		0.0014 ± 0.0001	1.5
ZnTCPP, H$_2$TCPP/TiO$_2$		0.50 ± 0.02	1.5
Ru-bpy with linker rod 1/TiO$_2$		0.035 ± 0.001	1.5
Ru-bpy with linker rod 2/TiO$_2$		0.023 ± 0.001	1.5
Ru-bpy/ZnO		0.012 ± 0.001	1.5
Ru-bpy/SnO$_2$, In$_2$O$_3$		0.058 ± 0.002	1.5

Information). In contrast to the emission decay in solution, there is a strong dynamic quenching in CdSe QD-sensitized TiO$_2$ film (Figure S3). As expected, the PL decay trace of CdSe QD-sensitized TiO$_2$ film is satisfactorily fitted by our model, as shown in **Figure 7**. This gives an electron transfer rate of 1.4 ns^{-1}, which is consistent with the report by Kongkanand et al.[20] This result is encouraging, and it extends the applicability of this model. We believe this would be helpful in developing deep insight into the nanointerfacial physics of CdSe QD-sensitized TiO$_2$ nanocrystalline films.

2.5. Quantitative Analysis and Simulation by Marcus Theory

With this conclusion, we could safely obtain the important parameters of the electron injection process from electron transfer (ET) rate coefficient, k_{ET}, such as electronic coupling constant, and free energy. One simple way to describe such a relationship is the classical Marcus expression, using a density of state of three-dimensional free electron gas for metal oxides conduction band (CB) edge, $\rho(E)$, as shown in Equations 2 and 3.[25]

$$k_{ET} = \frac{2\pi}{\hbar} \int dE \rho(E) \; |\bar{H}(E)^2| \; \frac{1}{\sqrt{4\pi\lambda k_B T}}$$
$$\times \exp\left[-\frac{(\lambda + \Delta G + E)^2}{4\lambda \; k_B T}\right] \tag{2}$$

$$\rho(E) = \frac{1}{2\pi^2}\left(\frac{2m^*}{\hbar^2}\right)^{3/2} E^{1/2} \tag{3}$$

here, $H(E)$ is the electronic coupling matrix element; λ is the reorganization energy; ΔG is the energy difference between the semiconductor CB and the excited state of the dyes; k_B is Boltzmann's constant; T is temperature; and m^* is the conduction band effective mass of nanocrystalline oxide, which for TiO$_2$ ≈ 10 m_0 based on Enright et al.[26] Integration over all values of E accounts for injection into all possible states in the metal oxide conduction band. All the driving force ΔG and satisfied k_{ET} are presented in Table 2. Under the assumption that the electronic coupling does not depend significantly on E, and the three kinds of dyes have same reorganization energy due to unique system structure, we got a value of $|H(E)|$ of approximately 44 cm^{-1} and λ of approximately 0.5 eV for a satisfactory result at room temperature $k_B T$ ≈ 26 meV (**Figure 8**). Our result shows that the organic dyes here have relative larger reorganization energy compared with that in the ruthenium-based dyes.[4] This may originate from the nature of these metal-free organic dyes, i.e., long molecular structure and large dipole, although the reorganization energy is usually influenced by the environment, such as the solvent, to a great extent. It is noted that the electron effective mass m^* of TiO$_2$ nanocrystals could not affect the value of reorganization energy, and a smaller m^* would give a larger average electronic coupling constant, though for bulk anatase crystals, m^* is only around 1 m_0.

www.MaterialsViews.com

ADVANCED
FUNCTIONAL
MATERIALS
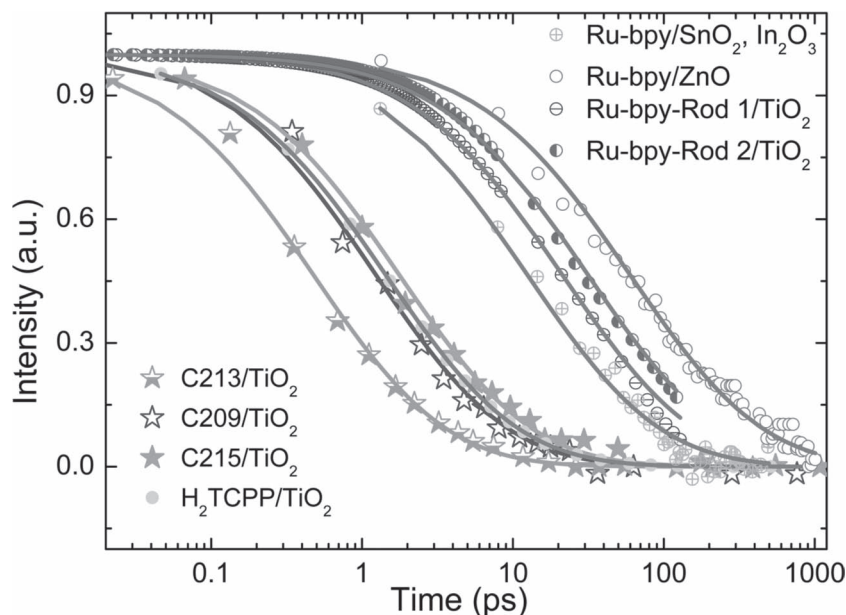www.afm-journal.de

FULL PAPER

Figure 6. Normalized electron injection dynamics for various kinds of dye-sensitized films used in this report. Solid lines are fitted by the model. Except the data of C209, C213, and C215, the other traces are extracted from the literature.[7–11] Note that the time axis is on an exponential scale.

2.6. The Effect of Heteroatom (O, S, and Se) in the Organic Dyes

Up to now, the role of the heteroatom (O, S, and Se) is clear, when adopting heterocycle as a linker connecting the donor with acceptor. From the device performance point of view, the electronegativity of the heteroatom indicates the change

Figure 7. Normalized emission decay trace (violet circle) for CdSe QD (3.0 nm) sensitized TiO₂ films. The pink solid line represents the kinetic fit by the model. The dotted line is the instrument response.

trend of open-circuit photovoltage, short-circuit photocurrent density, and external quantum efficiency (see Tables S1 and S2 in the Supporting Information for details). Herein, we have more attention towards deep insights into photoconversion physics. We found that the heteroatom itself in these organic dyes could not affect the important parameters describing the electron injection process, i.e., electronic coupling constant and reorganization energy; it only changes the molecular orbital. This could provide a new method to design optimal metal-free organic dye-sensitized photovoltaic devices by molecular engineering. For example, if the number of heterocycles is changed, it is reasonable to expect the only invariant is the electronic coupling constant, accompanied by red-shifted absorption, and reduced reorganization energy and driving force.

3. Conclusions

An electron injection picture has been clearly described: the electron injection in DSSCs is controlled by a nanointerfacial static inhomogeneous electronic coupling model. As we mentioned above, the applicability of this model is dependent on the distribution of surface states on metal oxide acceptors. Conversely, if some special treatment makes the electron injection kinetics depart from this model, it is possible that this could affect the distribution of electron coupling; such an observation would be very interesting from the point of view of both device design and fundamental physics. In addition, to our best knowledge, the discussion about electron coupling in such a large extension and time scale is still lacking. Here, all of the results presented provide strong experimental evidence for the concept that the complex nonexponential electron injection kinetics in these DSSCs and CdSe QD-sensitized films largely reflects the universal behavior resulting from the static inhomogeneity of the system, especially electronic coupling. Apparently, the observed kinetics are determined by driving force and reorganization energy. The result largely simplifies the complexity in DSSCs, and provides a reliable method to obtain useful information for designing an optimal metal-free organic dye-sensitized photovoltaic device by molecular engineering. It also will be helpful for study of the nanointerfacial physics in CdSe QD-sensitized films. Furthermore, in combination with charge recombination studies, determination of the relationship between device performance and dynamics analysis may not be far away; this would give a new insight into the fundamental physics in DSSCs.
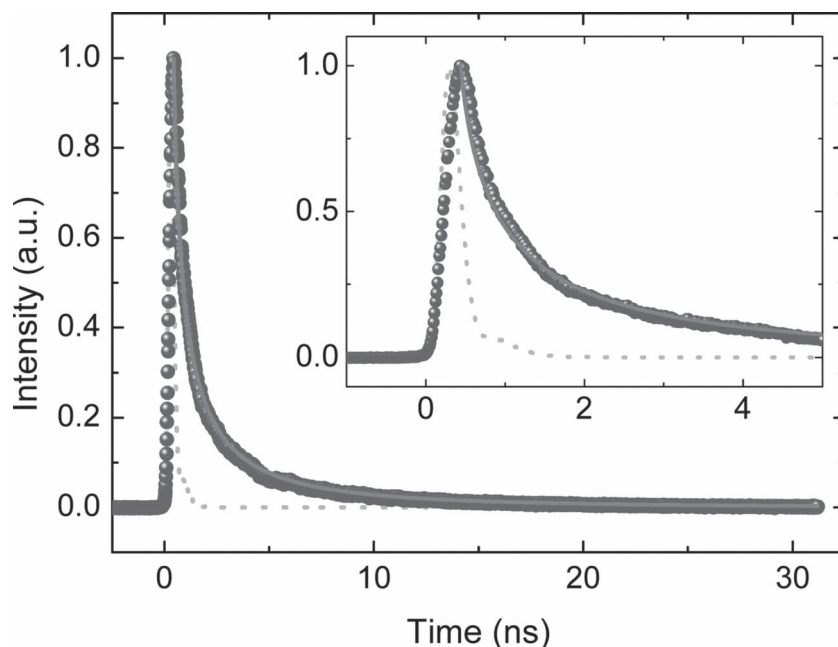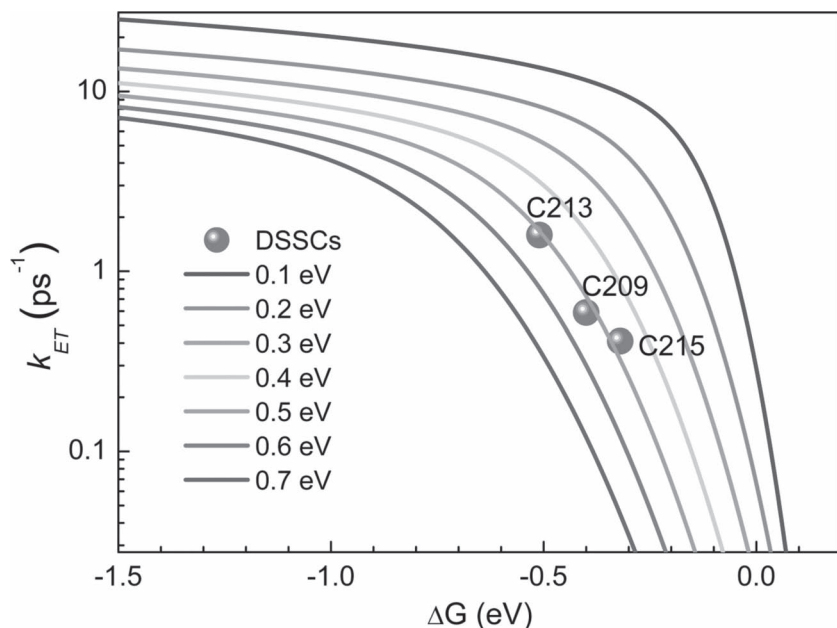
**ADVANCED
FUNCTIONAL
MATERIALS**

www.afm-journal.de

*Materials
Views*

www.MaterialsViews.com

FULL PAPER

Figure 8. Measured electron injection rate for three kinds of metal-free organic DSSCs and predicted ET rate as a function of driving force under different reorganization energy.

4. Experimental Section

Dye-Sensitized Devices and Films: All dye-sensitized films and devices used in this report were provided by Wang Peng's group, which are fabricated and characterized as described in the literature.[13] Typically, a cycloidal TiO_2 electrode (approximately 0.28 cm^2) on fluorine-doped SnO_2 (FTO) conducting glass was immersed into a dye solution containing C209, C213, and C215 sensitizer (300 μM) and Cheno (2 mM) in acetonitrile for 5 h. After washing with acetonitrile and dried, the sensitized titania electrode was assembled with a thermally platinized FTO electrode. The electrodes were separated by a 35 μm thick hot-melt gasket and sealed up by heating. The internal space was filled with a liquid electrolyte. Finally, the electrolyte-injecting hole on the counter electrode glass substrate was sealed, and the resulted samples were used for further steady-state and transient measurements. Based on electrochemical measurements, it provided the information of dyes' lowest unoccupied molecular orbital (LUMO) and highest occupied molecular orbital (HOMO) in solution.

CdSe QD-Sensitized Films: The CdSe QDs were synthesized by a modified literature method.[27] A typical synthesis of CdSe nanocrystals was as follows. A mixture of CdO (77.04 mg), oleic acid (677.9 mg), and technological-grade octadecene (ODE, 8.1 g) was heated to 250 °C to get a clear solution. After cooling down to room temperature, 1.5 g trioctylphosphine oxide (TOPO) and 1.5 g hexadecylamine (HDA) were added, and the mixture was heated to 340 °C again. A mixture of 2.9 g 10 wt-% Se-trioctylphosphine (TOP) solution and 1.1 g of ODE was quickly injected into this hot solution, and then the reaction mixture was allowed to cool to 310 °C for the growth of CdSe nanocrystals. The reaction was stopped when the desired nanocrystal size was reached. The synthesis was carried out under nitrogen. Ligand exchange by butylamine was performed following a recently reported method.[28] After the ligand exchange, a CdSe QDs solution with 0.5 mL butylamine and 2.5 mL toluene was stored for sensitization. The CdSe QD-sensitized film was prepared by exposing a nanocrystalline TiO_2 film with 20 nm particle size and 2.6 μm thickness to the stored butylamine-capped CdSe QDs solution in darkness. The exposure time was 48 h. The CdSe QD-sensitized film was washed twice with toluene. Finally, a fresh CdSe QD-sensitized film was used for experiment when it was dry.

Femtosecond Transient Absorption (TA) Setup: The TA setup[29,30] consisted of 400 nm pump pulses doubled from 800 nm laser pulses (approximately 100 fs duration, 250 Hz repetition rate) generated from a mode-locked Ti:sapphire laser/amplifier system (Spectra-Physics) and broadband (450–850 nm) white-light probe pulses generated from 5 mm thick sapphire substrate. The relative polarization of the pump and the probe beams was set to the magic angle. The TA data were collected by a fiber-coupled spectrometer connected to a computer. The group velocity dispersion of the transient spectra was compensated by a chirp program.

Time-Resolved Photoluminescence: Sub-picosecond time-resolved emissions were measured by the femtosecond fluorescence upconversion method.[31,32] A Nd:YVO laser (Millennia, Spectra Physics) was used to pump a Ti:Sapphire laser (Tsunami, Spectra Physics). Its output seeded a regenerative amplifier (RGA, Spitfire, Spectra Physics). The output of the amplifier of 1.5 mJ pulse energy, 100 fs pulse width, at 800 nm wavelength was split into two equal parts; the second harmonic (400nm) of one beam was focused in the sample as excitation. The resulted fluorescence was collected and focused onto a 1 mm thick BBO crystal with a cutting angle of 35°. The other part of the RGA output was sent into an optical delay line and served as the optical gate for the upconversion of the fluorescence. The generated sum frequency light was then collimated and focused into the entrance slit of a 300 mm monochromator. A UV-sensitive photomultiplier tube 1P28 (Hamamatsu) was used to detect the signal. The electrical signal from the photomultiplier tube was summed by a digital oscilloscope. The FWHM of instrument response function was about 400 fs. The probe wavelength was chosen at the peak of the emission spectra in the film. All the measurements were performed at room temperature. Pump-power-dependent measurements were carried out. In the acceptable range, no pump intensity dependent dynamics were observed. Nanosecond fluorescence lifetime experiments were performed by the time-correlated single-photon counting (TCSPC) system under right-angle sample geometry. A 405 nm picosecond diode laser (Edinburgh Instruments EPL375, repetition rate 2 MHz) was used to excite the samples. The fluorescence was collected by a photomultiplier tube (Hamamatsu H5783p) connected to a TCSPC board (Becker&Hickel SPC-130). The time constant of the instrument response function (IRF) was about 300 ps.

[1] B. O'Reagan, M. Grätzel, *Nature* **1991**, *353*, 737.
[2] Q. J. Yu, Y. H. Wang, Z. H. Yi, N. N. Zu, J. Zhang, M. Zhang, P. Wang, *ACS Nano* **2010**, *4*, 6032.
[3] M. Gratzel, *J. Photochem. Photobiol. C* **2003**, *4*, 145.
[4] J. R. Durrant, S. A. Haque, E. Palomares, *Coord. Chem. Rev.* **2004**, *248*, 1247.
[5] S. Ardo, G. J. Meyer, *Chem. Soc. Rev.* **2009**, *38*, 115.

[6] H. Y. Wang, S. Lin, J. P. Allen, J. C. Williams, S. Blankert, C. Laser, N. W. Woodbury, *Science* **2007**, *316*, 747.

[7] Y. Trachibana, S. A. Haque, I. P. Mercer, J. R. Durrant, D. R. Klug, *J. Phys. Chem. B* **2000**, *104*, 1198.

[8] M. Myahkostupov, P. Piotrowiak, D. Wang, E. Galoppini, *J. Phys. Chem. C* **2007**, *111*, 2827.

[9] J. B. Asbury, Y. Q. Wang, T. Q. Lian, *J. Phys. Chem. B* **1999**, *103*, 6643.

[10] X. Ai, N. A. Anderson, J. C. Guo, T. Q. Lian, *J. Phys. Chem. B* **2005**, *109*, 7088.

[11] J. C. Guo, D. Stockwell, X. Ai, C. X. She, N. A. Anderson, T. Q. Lian, *J. Phys. Chem. B* **2006**, *110*, 5238.

[12] S. A. Haque, E. Palomares, B. M. Cho, A. N. M. Green, N. Hirata, D. R. Klug, J. R. Durrant, *J. Am. Chem. Soc.* **2005**, *127*, 3456.

[13] R. Z. Li, X. J. Lv, D. Shi, D. F. Zhou, Y. M. Cheng, G. L. Zhang, P. Wang, *J. Phys. Chem. C* **2009**, *113*, 7469.

[14] R. Z. Li, J. Y. Liu, N. Cai, M. Zhang, P. Wang, *J. Phys. Chem. B* **2010**, *114*, 4461.

[15] R. Z. Li, D. X. Liu, D. F. Zhou, Y. S. Shi, Y. H. Wang, P. Wang, *Energy Environ. Sci.* **2010**, *3*, 1765.

[16] J. Y. Liu, R. Z. Li, X. Y. Si, D. F. Zhou, Y. S. Shi, Y. H. Wang, X. Y. Jing, P. Wang, *Energy Environ. Sci.* **2010**, *3*, 1924.

[17] Y. Tachibana, I. V. Rubtsov, I. Montanari, K. Yoshihara, D. R. Klug, J. R. Durrant, *J. Photochem. Photobiol. A* **2001**, *142*, 215.

[18] A. S. Huss, A. Bierbaum, R. Chitta, D. J. Ceckanowicz, K. R. Mann, W. L. Gladfelter, D. A. Blank, *J. Am. Chem. Soc.* **2010**, *132*, 13963.

[19] I. Robel, M. Kuno, P. V. Kamat, *J. Am. Chem. Soc.* **2007**, *129*, 4136.

[20] A. Kongkanand, K. Tvrdy, K. Takechi, M. Kuno, P. V. Kamat, *J. Am. Chem. Soc.* **2008**, *130*, 4007.

[21] H. N. Ghosh, J. B. Asbury, T. Q. Lian, *J. Phys. Chem. B* **1998**, *102*, 6482.

[22] M. Hilgendorff, V. Sundström, *Chem. Phys. Lett.* **1998**, *287*, 709.

[23] P. V. Kamat, *Chem. Rev.* **1993**, *93*, 267.

[24] W. W. Yu, L. H. Qu, W. Z. Guo, X. G. Peng, *Chem. Mater.* **2003**, *15*, 2854.

[25] N. A. Anderson, T. Q. Lian, *Annu. Rev. Phys. Chem.* **2005**, *56*, 491.

[26] B. Enright, D. Fitzmaurice, *J. Phys. Chem.* **1996**, *100*, 1027.

[27] W. W. Yu, X. G. Peng, *Angew. Chem., Int. Ed.* **2002**, *41*, 2368.

[28] N. Fuke, L. B. Hoch, A. Y. Koposov, V. W. Manner, D. J. Werder, A. Fukui, N. Koide, H. Katayama, M. Sykora, *ACS Nano* **2010**, *4*, 6377.

[29] L. Wang, H. Y. Wang, B. R. Gao, L. Y. Pan, Y. Jiang, Q. D. Chen, W. Han, H. B. Sun, *IEEE J. Quantum Electron.* **2011**, *47*, 1177.

[30] L. Y. Pan, Y. L. Zhang, H. Y. Wang, H. Liu, J. S. Luo, H. Xia, L. Zhao, Q. D. Chen, S. P. Xu, B. R. Gao, L. M. Fu, H. B. Sun, *Nanoscale* **2011**, *3*, 2882.

[31] B. R. Gao, H. Y. Wang, Y. W. Hao, L. M. Fu, H. H. Fang, Y. Jiang, L. Wang, Q. D. Chen, H. Xia, L. Y. Pan, Y. G. Ma, H. B. Sun, *J. Phys. Chem. B* **2010**, *114*, 128.

[32] H. Wang, H. Y Wang, B. R. Gao, L. Wang, Z. Y. Yang, X. B. Du, Q. D. Chen, J. F. Song, H. B Sun, *Nanoscale* **2011**, *3*, 2280.